Measurement of the ^{20}F half-life

M. Hughes,[1,2] E. A. George,[3] O. Naviliat-Cuncic,[1,2,*] P. A. Voytas,[3] S. Chandavar,[2] A. Gade,[1,2]
X. Huyan,[1,2] S. N. Liddick,[2,4] K. Minamisono,[1,2] S. V. Paulauskas,[2] and D. Weisshaar[2]
[1]*Department of Physics and Astronomy, Michigan State University, East Lansing, 48824 Michigan, USA*
[2]*National Superconducting Cyclotron Laboratory, Michigan State University, East Lansing, 48824 Michigan, USA*
[3]*Department of Physics, Wittenberg University, Springfield, 45504 Ohio, USA*
[4]*Department of Chemistry, Michigan State University, East Lansing, 48824 Michigan, USA*

(Received 23 November 2017; published 29 May 2018)

The half-life of the ^{20}F ground state was measured using a radioactive beam implanted in a plastic scintillator and recording $\beta\gamma$ coincidences together with four CsI(Na) detectors. The result, $T_{1/2} = 11.0011(69)_{\rm stat}(30)_{\rm sys}$ s, is at variance by 17 combined standard deviations with the two most precise results. The present value revives the poor consistency of results for this half-life and calls for a new measurement, with a technique having different sources of systematic effects, to clarify the discrepancy.

DOI: 10.1103/PhysRevC.97.054328

I. INTRODUCTION

The particular decay properties of the $A = 20$ isospin triplet have attracted considerable attention as being advantageous for performing correlation measurements in β decay that test the strong form of the principle of conservation of the vector current [1]. The comparison of ft values from ^{20}F and ^{20}Na was used for tests of mirror symmetry and searches for second-class currents [2]. In nuclear astrophysics, the lifetime of ^{20}F plays a role in the evolution of stars with masses in the range $8-12M_{\odot}$ which become electron-capture supernovae [3]. The collapse is triggered by the loss of electron pressure support via the sequence ^{20}Ne$(e^-,\nu)^{20}$F$(e^-,\nu)^{20}$O on the very abundant ^{20}Ne nuclear species [4]. The precision requirements on the ^{20}F lifetime for these two domains are vastly different. Whereas for astrophysical calculations of electron capture rates a relative uncertainty of 10% would be sufficient [5], mirror symmetry tests will ultimately be limited by the accuracy in the determination of the statistical rate function, f. For the most favorable decays, this can be determined with an accuracy of few 10^{-4} [6].

The β decay of ^{20}F ($E_{\rm max} = 5.4$ MeV) occurs almost exclusively (99.99%) to the first excited state in ^{20}Ne which subsequently decays with the emission of a 1.63-MeV γ ray. The ^{20}F lifetime was therefore measured by either detecting β particles in singles, γ rays in singles, or both in $\beta\gamma$ coincidences. The adopted value for the ^{20}F half-life, $T_{1/2} = 11.163(8)$ s [7], arises from a single measurement [8] which detected γ rays in singles with a Ge(Li) detector. The value is consistent with a previous result [9] obtained by counting β particles in singles using a magnetic spectrometer. However, the adopted value [7] does not reflect the spread among the values previously measured. Figure 1 shows results from measurements of the half-life having a total uncertainty σ_i, which is at most 10 times larger than the most precise result of Ref. [8]. The red curve is a sum of Gaussians, weighted by $(1/\sigma_i^2)$, and is dominated by the two most precise results. There appears to be no correlation between the reported values and the experimental techniques, whether these used β particles in singles [9–11], γ rays in singles [8,12–14], or $\beta\gamma$ coincidences [15]. The short description in Ref. [2] suggests that the measurements were carried out with β particles and γ rays in singles, over different time intervals. The poor statistical consistency of the results can be quantified by a fit of the nine values with a constant, which gives $T_{1/2} = 11.1521(58)$ s with $\chi^2/\nu = 37.5$.

The present work reports a high statistics measurement of the ^{20}F half-life performed by counting $\beta\gamma$ coincidences. The experiment was carried out in the framework of β-decay studies of ^{20}F. Although the settings of the main experiment, in particular the duration of the decay time windows, were not optimized for the half-life measurement, the conditions were particularly clean in terms of background, and a number of ancillary diagnostics were available to control possible systematic effects. A preliminary progress report of the work reported here was presented elsewhere [16].

II. EXPERIMENTAL CONDITIONS

The experiment was performed at the National Superconducting Cyclotron Laboratory (NSCL) at Michigan State University. A primary ^{22}Ne beam was accelerated to 150 MeV per nucleon by the Coupled Cyclotron Facility and impinged on a 188-mg/cm^2-thick Be target where the ^{20}F was produced by projectile fragmentation. The secondary beam was analyzed by the A1900 fragment separator [17] and was directed to the experimental area. During beam tuning, the beam purity was measured to be 99.4% with a 4-mm-wide aperture at the focal plane of the A1900 separator. The only observed radioactive contaminant was ^{19}O, at a level of 0.23%. During regular measurement runs, the aperture at the focal plane of

*naviliat@nscl.msu.edu

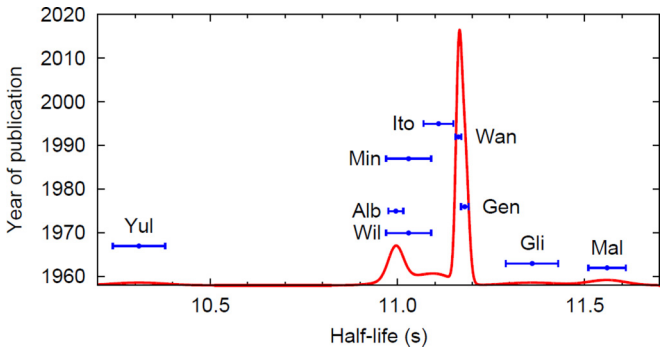

FIG. 1. Measurements of the ^{20}F half-life prior to the present work along with their year of publication. The red curve is an ideogram obtained from a sum of Gaussians centered at the mean values and having a weight $(1/\sigma_i^2)$, where σ_i is the uncertainty of the measurement. The labels correspond to Mal [15], Gli [12], Yul [13], Wil [2], Alb [10], Gen [9], Min [11], Wan [8], and Ito [14].

the fragment separator was reduced to 1 mm (±0.5 mm), and the amount of the ^{19}O contaminant was reduced to the level of 0.06%.

In the experimental area, the ^{20}F ions exited the beam pipe through a 75-μm-thick Zr vacuum window and were implanted into a O7.6 × 7.6 cm^2 EJ-200 polyvinyltoluene (PVT) plastic scintillator detector (Fig. 2). The beam energy before the PVT detector was 132 MeV/nucleon. Beam transport calculations using the LISE++ code [19] indicated that the beam was implanted at a mean depth of 3.02 cm inside the PVT and produced a range straggling ±0.6 mm wide around the mean depth position. The PVT was surrounded by four 7.6 × 7.6 × 7.6 cm^3 CsI(Na) modules from the CAESAR array [18] for the detection of the γ rays. The transverse beam dimensions were measured with a position sensitive parallel plate avalanche counter (PPAC), placed in vacuum 40 cm upstream from the implantation detector and removed during regular runs. The beam shape observed by the PPAC was elliptical, 8-mm wide and 6-mm high at full width tenth of maximum (FWTM). Between the PPAC and the implantation detector the beam

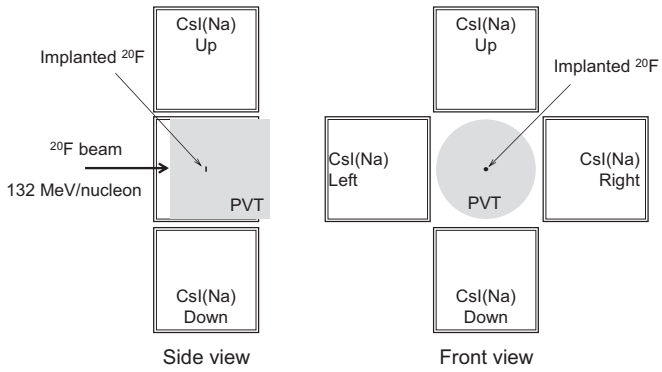

FIG. 2. Layout of the experimental setup showing a side view (left) and front view (right) of the detector arrangement around the position where the beam stops. The PVT detector is offset downstream so that the position of the implanted ^{20}F is centered relative to the CsI(Na) detectors.

was convergent. From the beam transport magnification and the measurements in the PPAC, the actual size of the beam spot at the stopping location was deduced to be 3.6 mm in the horizontal and 3.4 mm in the vertical directions (FWTM). The range of 5.4-MeV electrons in PVT is 2.75 cm. This means that β particles from ^{20}F decay cannot escape from the detector in any direction.

A pulse generator was used to monitor the gain stability of the PVT detector. The generator drove an external light emitting diode (LED) linked to two parallel outputs via optical fibers. One of the outputs was connected to a Plexiglas ring which served to couple the PVT detector to its photomultiplier tube (PMT) and the other one was directed to an external Si PIN photodiode. The generator was operated at a trigger rate of 500 Hz and produced two pulses of slightly different amplitude per trigger, both well above the β-spectrum endpoint, and separated by 136 μs.

The CsI(Na) and PVT detectors were calibrated using, respectively, the γ lines and the Compton edges from ^{22}Na, ^{60}Co, and ^{137}Cs sources, and the responses were found to be linear over the energy range covered by the sources. The energy resolution of the four CsI(Na) detectors at 1.63 MeV was between 7.3%–7.9% FWHM. In the absence of beam, the ambient background rate of the CsI(Na) detectors was about 250 counts per second (cps) and was less than 30 cps for the PVT detector.

III. DATA ACQUISITION AND MEASUREMENT SEQUENCE

The data acquisition was based on the implementation of the digital NSCL system [20] using three 250 megasamples per second Pixie-16 digitizing modules from the XIA company. The signals from the five detectors, i.e., the PVT and the four CsI(Na), were sent to the first module. The second module received the five signals from the PPAC, and one signal from a Si detector used during beam tuning. Both Pixie modules also received signals associated with the beam-on start, the beam-off start, an additional 100-Hz pulser, and the signal from the Si PIN photodiode for monitoring. For each input channel in these two modules, the digitizer provided the time stamp and an energy conversion using a trapezoidal filter [20]. The third Pixie module was used to digitize the waveforms from the PVT detector over a 400-ns-wide window. The waveforms have been used to check the energy filter of the digitizer but have otherwise not been specifically exploited for the half-life measurement reported here. The clock source generating the time stamping and signal sampling in the Pixie-16 modules uses an EPSON SGR-8002JC-PCB programmable crystal oscillator which has a frequency stability of $\pm 5 \times 10^{-5}$ within a temperature range from $-20\,^{\circ}$C to $70\,^{\circ}$C.

The Pixie modules continuously digitize the incoming waveforms but do not record information until a threshold is crossed. Once the threshold is crossed, the FPGAs in the Pixie system report an estimate of the event energy based on particular sums of the samples of the waveform at the input, following a trapezoidal filtering of the signal. From the time the threshold is crossed until the estimate is finished, no further triggers are acknowledged. However, if the input waveform is

TABLE I. Experimental conditions for the runs within the sets. For each set, the table lists the duration of the beam-on and beam-off intervals, the high-voltage bias on the PVT, the setting of the high-voltage inhibit, the primary beam intensity, the number of runs, and the total number of cycles.

Set	Beam on (s)	Beam off (s)	PVT HV (V)	HV inhibit	Beam intensity (nA)	Runs	Total cycles
1	1.67	30	−975	Off	30	9	915
2	1.67	30	−975	Off	93	2	77
3	1.67	30	−975	On	30	9	965
4	1.67	30	−975	On	93	11	1059
5	1.67	30	−856	On	93	10	1066
6	1.00	60	−800	On	93	1	63
7	1.10	20	−780	On	93	10	1604

from the close overlap of more than one signal, the presence of a second signal will affect the value of the resulting energy estimate. This is essentially a pile-up event and the value of the resulting energy estimate depends on the parameters of the trapezoidal filter and on the relative timing between the signals. The two signals are reported as one with an energy estimate somewhere between that of the first signal alone and the sum of the two signals, depending on the time difference between the signals. The contribution of such pile-up events depend on the particular energy cuts used and on the shape of the energy spectrum. In the analysis described below, events lost from the summing region were dealt with through the dead-time correction and those added to the summing region were dealt with through a pile-up correction. There is no other known event loss in this system at the rates of the experiment.

The time structure of a cycle consisted of a "beam-on" interval, of 1.0, 1.1, or 1.67 s, during which the ^{20}F beam was implanted into the PVT detector, followed by a "beam-off" interval of 20, 30, or 60 s to measure the decay. The beam chopping was performed by dephasing the radio-frequency signal of one of the cyclotrons. To reduce gain shifts in the PVT PMT resulting from the large dynode currents during beam implantation, the PMT HV was reduced (HV Inhibit) by a factor of 2 during the implantation duration of the cycle. This was applied for most of the runs (Table I). Other parameters such as the primary ^{22}Ne^{10+} beam intensity, the durations of the beam-on and beam-off windows, the high voltage on the PVT PMT and the inhibit of the PMT high voltage, were changed during the experiment to check for possible systematic effects. The conditions are summarized in Table I and resulted in seven sets of runs listed in chronological order. Most of the runs in each set were 1-h long.

For the runs with a low primary beam intensity of 30 nA (electric), the singles counting rates 2 s after beam-off were about 3500 cps and 480 cps for the PVT and CsI(Na) detectors, respectively. For runs with the high beam intensity of 93 nA, these rates were typically 11 500 cps and 1200 cps.

IV. SAMPLE SPECTRA

Figure 3 shows a two-dimensional histogram for a single run from set 7, of the energy deposited in the CsI(Na)-Right detector versus the energy in the PVT detector, recorded during the beam-off interval. The events were required to be within a 400-ns-long software event window generated by the first arriving signal. The β distribution associated with the 1.63-MeV γ coincidences is clearly visible. There is no indication of transitions from contaminants giving rise to γ rays with energies larger than 1.63 MeV. The analysis of events which are associated with the 0.511-MeV peak indicated that those arise mainly from two β^+ emitters having distinct half-lives and end-point energies. Their properties are consistent with those of ^{10}C and ^{11}C decays, which can be produced by reactions on ^{12}C in the PVT. The production of ^{10}C was confirmed by requiring a fourfold coincidence between the implantation detector, two back-to-back CsI(Na) detectors to record pairs of 511-keV photons, and a third CsI(Na) detector to identify the 718-keV γ ray from ^{10}B. The identification of these distributions with ^{10}C and ^{11}C was furthermore confirmed by a test in which the PVT detector was replaced by a CsI(Na) detector and where no such distributions were observed.

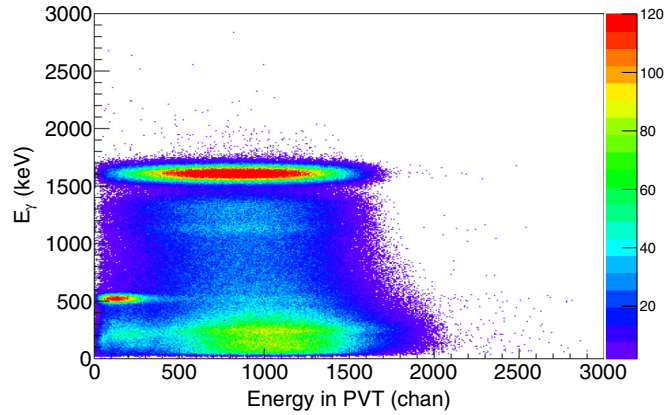

FIG. 3. Two-dimensional histogram of the energy in the CsI(Na)-Right detector versus the energy deposited in the PVT detector. See text for details.

Figure 4 shows the projection of Fig. 3 on the γ-energy (vertical) axis, without any condition on the PVT energy. The vertical lines show mean positions of cuts around the 1.63-MeV peak which were varied in the analysis to test the stability of the

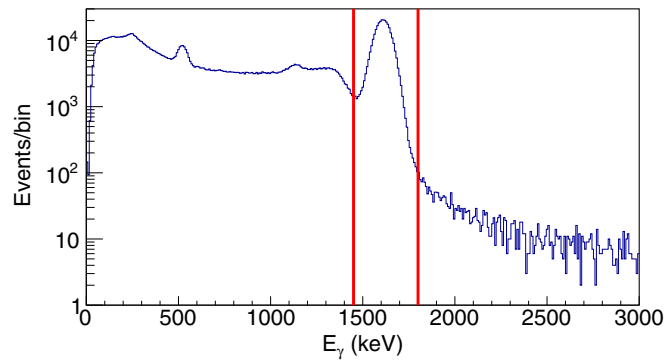

FIG. 4. Energy spectrum of γ rays detected in coincidence with a signal in the PVT implantation detector. The vertical lines indicate the mean positions of the cuts applied for this detector.

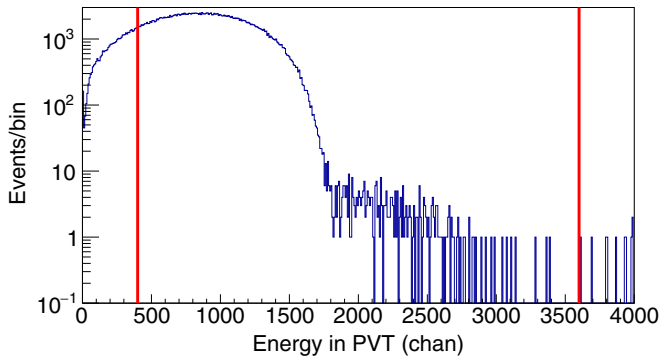

FIG. 5. Energy deposited in the PVT detector recorded in coincidence with a signal in one of the four CsI(Na) detectors and gated around the 1.63-MeV peak. The vertical lines indicate the reference positions of cuts used for the final analysis in data set 6.

results. Towards lower energies from the peak, the spectrum shows the Compton edge and the single escape peak. Monte Carlo simulations indicated that the events observed towards higher energies are dominated by bremsstrahlung produced by electrons in the PVT detector. Figure 5 shows a projection of Fig. 3 on the PVT energy, with the cuts shown in Fig. 4. The vertical lines in Fig. 5 indicate the position of the cuts on the PVT energy that were also varied during the analysis to test the stability of the results.

Decay histograms were built from events in the 1.63-MeV peak window detected in coincidence with the PVT detector. Each CsI(Na) detector produces a statistically independent decay spectrum resulting in 208 spectra from 52 runs distributed among the seven sets of Table I. Cuts were also applied to the time difference between the PVT and the CsI(Na) signals such as to select events around the prompt peak (Fig. 6). All events in Fig. 6 satisfy by construction the energy cuts on the β and γ spectra. Events located left from the peak correspond to accidental coincidences from ambient background. The larger level of events located right from the prompt peak is produced by $\beta\gamma$ coincidences between time uncorrelated signals associated with two decays in the PVT detector occurring within the dead-time window of the PVT

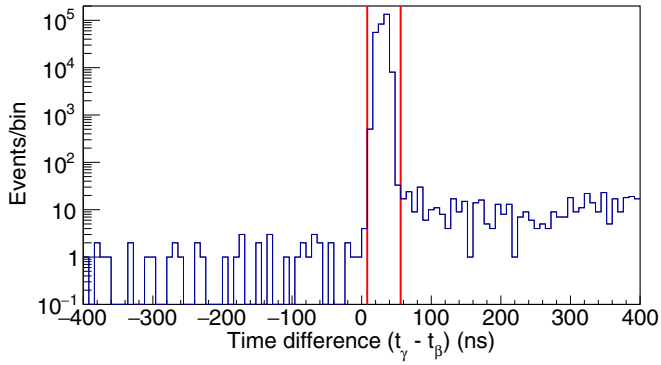

FIG. 6. Time difference between a signal from the PVT detector and a signal from the CsI(Na)-Right detector obtained from events satisfying the β and γ energy cuts. The vertical lines indicate the narrowest cuts, ± 24 ns around the prompt peak, used in the analysis.

channel. For these events, the second β signal is dead-time suppressed by the first; The γ ray of the second decay falls within the energy window of a CsI(Na) module and is then detected in coincidence with the first β. The γ ray associated with the first decay is either detected as a Compton event by one of the other three CsI(Na) detectors or goes undetected. More details are given in Sec. VI C.

Two types of energy cut methods were used on the energy spectra, one with fixed positions for each set of runs listed in Table I and another where the cuts were determined individually for each run, relative to the position of the 1.63-MeV peak centroid and to the endpoint of the β spectrum. This second approach accounted for gain drifts between runs of a given set such as to have more similar conditions for each run. Such adaptive cuts do not account, however, for rate dependent gain shifts that can occur during the decay window. Both methods gave consistent results.

With the cuts around the γ peak (Fig. 4), the lower cut in the β energy spectrum above the ^{10,11}C contaminants and the cuts around the peak in the time difference spectrum (Fig. 6), the typical coincidence rates between the PVT detector and one CsI(Na) detector were 35 cps for the runs with the reduced beam intensity and 120 cps for the runs with higher beam intensity. The typical average ambient background coincidence rate with the same cuts was 1.5×10^{-3} cps.

V. DATA ANALYSIS

For each CsI(Na) detector, the decay spectrum was built after imposing the cuts on the γ energy spectrum, on the β energy spectrum, and on the time difference between the β and γ signals. Events were binned every 0.25 s. To avoid edge effects, the histogram was fit from 1.5 s after the beginning of the beam-off window up to 1.5 s before the end of the window. The time used in the decay spectrum was obtained from the time stamp of the PVT detector signal relative to the time stamp of the beam-off signal. The fitting function was of the form,

$$f(t) = a \exp(-t \ln 2 / T_{1/2}), \tag{1}$$

with a and $T_{1/2}$ as free parameters. The effect of accidental coincidences from ambient background is discussed in Sec. VI D. The parameters were determined using the log-likelihood method. Fits of comparable quality were obtained before and after the dead-time corrections of decay spectra.

The fit of a dead-time corrected decay spectrum for the CsI(Na)-Up detector, with a 60-s beam-off window, is shown in Fig. 7. The associated residuals are defined as $R_i = [f(t_i) - n_i]/\sqrt{n_i}$, with n_i the number of counts in bin i. The other parameters for this particular run are given in Table I.

The values of half-lives resulting from fits having a p value smaller than 0.05 were excluded from the data sample. The fraction of such fits was 0.06 and they are distributed over the full set of runs and among the four detectors. This fraction is consistent with expectations from pure statistical fluctuations. To illustrate the weight of the data sets, the results of the half-life for each set, averaged over all four detectors, are presented in Table II. For reasons explained in Sec. VI E, sets 1 and 2 were excluded from the data sample to calculate the final result.

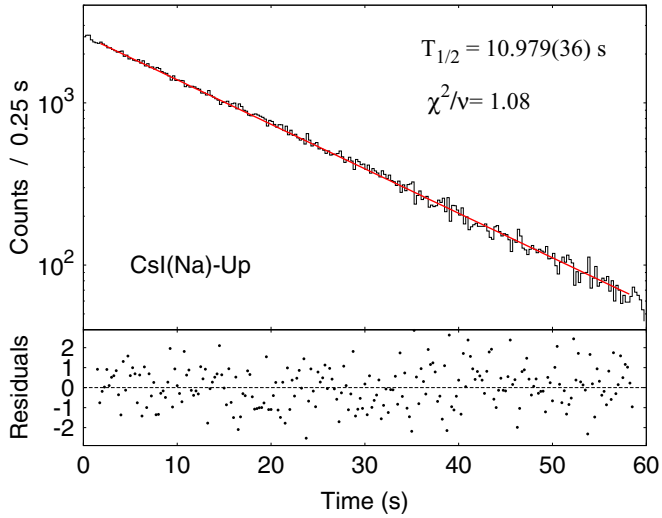

FIG. 7. (Upper panel) Decay spectrum from the CsI(Na)-Up detector (black histogram) and fitted function (red line). (Lower panel) Normalized residuals from the fit.

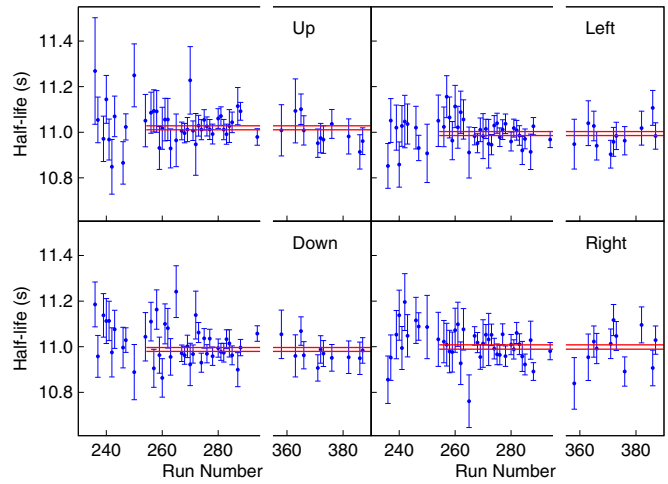

FIG. 8. Values of the half-lives obtained from fits of the decay histograms for the four CsI(Na) detectors as a function of the run number. The horizontal bands indicate the $\pm 1\sigma$ limits of the fits from data sets 3 to 7.

From the remaining sets, it is clear that sets 4 and 5 have the largest weight.

Figure 8 shows all individual values of half-lives for the four detectors and for all runs after dead-time correction. The horizontal bands indicate for each detector the $\pm 1\sigma$ (statistical) limits of the fit of values from sets 3 to 7 having a p value larger than 0.05. The values are summarized in Table III along with their normalized χ^2.

A fit to the four values in Table III gives the tabulated mean and χ^2/ν, with a p value $= 0.062$. A fit of all results from sets 3 to 7, without grouping them first by detector, gives $T_{1/2} = 11.0001(44)$ s with $\chi^2/\nu = 0.87$ and a p value $= 0.87$. If the fits with p values smaller than 0.05 were included in the sample, the half-life would change by -3×10^{-4} s. To account for the spread in the values obtained when grouping them by detectors, which is due primarily to the Up detector, the statistical uncertainty on the mean value was increased by $\sqrt{\chi^2/\nu} = 1.56$ in the final result.

TABLE II. Dead-time corrected half-lives obtained for each data set from the fits of decay spectra, averaged over the four CsI(Na) detectors. For each run, the lower PVT energy cut was set just above the carbon contaminants and the narrowest cuts were used on the relative time between the β and the γ signals.

Set	$T_{1/2}$ (s)	χ^2/ν
1	11.0303(175)	0.88
2	11.0100(242)	1.06
3	11.0258(152)	0.94
4	11.0033(71)	0.69
5	10.9987(77)	1.12
6	10.9735(253)	0.05
7	10.9869(108)	0.74

VI. SYSTEMATIC EFFECTS

A. Dead-time correction

The shortest time differences between consecutive signals, as measured from the time stamps, were $\tau_\beta = 464$ ns and $\tau_\gamma = 656$ ns for, respectively, the PVT and CsI(Na) channels. These determine the effective dead times of the system for these channels. The time window of the software events, of 400 ns, was chosen to be smaller than both of those effective dead times. The measured coincidence rates, $r^m_{\beta\gamma}$, at a given time after beam-off were corrected according to

$$r^c_{\beta\gamma} = \frac{1}{1 - r_\beta \tau_\beta} \cdot \frac{1}{1 - r_\gamma \tau_\gamma} r^m_{\beta\gamma}, \qquad (2)$$

where r_β is the singles rate in the PVT detector including events from the pulser and r_γ is the singles rate in the associated coincident CsI(Na) detector. To check for effects of intensity variations during a run, the correction was applied to rates measured cycle by cycle as well as to averaged rates measured over a run. Both methods gave consistent results because the data were taken under stable beam conditions.

TABLE III. Dead-time corrected half-lives obtained from fits of values from sets 3 to 7 for the four CsI(Na) detectors with their corresponding normalized χ^2. For each run, the lower PVT energy cut was set just above the carbon contaminants and the narrowest cuts were used on the relative time between the β and γ signals.

Detector	$T_{1/2}$ (s)	χ^2/ν
Up	11.0195(88)	0.62
Left	10.9944(87)	0.67
Down	10.9880(85)	1.02
Right	10.9987(95)	1.08
Mean	10.9999(44)	2.44

TABLE IV. Systematic effects considered in the error budget, with the size of the effect on the half-life and the adopted uncertainty. See text for details on the variations responsible for the corrections and uncertainties.

Source	Correction (ms)	Uncertainty (ms)
Dead-time correction	0.00[a]	0.24
Oscillator stability	0.00	0.80
Uncorrelated events	1.47	1.47
Lower CsI(Na) cut	0.00	0.15
Upper CsI(Na) cut	0.00	0.05
Lower PVT cut	0.00	2.32
Binning	−0.30	0.30
Systematic correction	1.17	2.89

[a]The mean value quoted in Table III includes the dead-time correction.

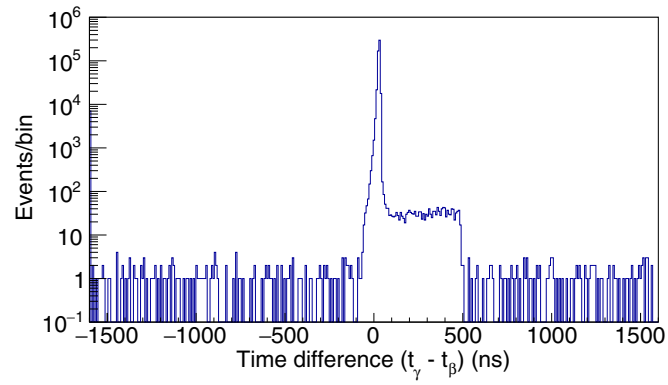

FIG. 9. Time difference between a signal from the PVT detector and a signal from the CsI(Na)-Left detector. This is similar to Fig. 6 but without the 400-ns time condition between signals.

The relative size of the correction on the rates is about 6×10^{-3} at the beginning of the decay histogram for the runs with the largest beam intensity. The comparison between the fitted values obtained with and without dead-time corrections showed that the central value of the half-life changed by 6–8 ms for the runs at low primary beam intensity and by 31–36 ms for the runs at high primary beam intensity. These corrections have been included in the results reported in Tables II and III. Because of the 250-MHz sampling rate of the digitizers, there is an uncertainty of ±4 ns on the measured dead times. This induces a systematic uncertainty of 0.24 ms on the half-life as listed in Table IV.

B. Oscillator stability

As indicated in Sec. III, the crystal oscillator has a stability of $\pm 5 \times 10^{-5}$. When applied to the duration of the decay window, such a stability was observed to produce a variation of ±0.80 ms on the extracted half-life.

C. Pile-up effects

The dead-time correction made through Eq. (2) accounts for losses of coincidence events from either β or γ suppressions by a previously occurring event within the dead-time window of the data acquisition channel. This corrects then for events removed from the energy window defined by the cuts in Fig. 4. However, this energy window can also receive events from the pile-up of two γ rays having smaller energies or from a γ ray detected in coincidence with a β from a previously occurring event.

As explained in Sec. V, when two ^{20}F decay events occur during the dead time of the β channel they can give rise to the time uncorrelated events appearing at later times (right) from the prompt peak in Fig. 6. For clarity, Fig. 9 displays a spectrum of the relative time between the PVT and a CsI(Na) but which was built without imposing the 400-ns-wide software condition between events. The total duration of the plateau having a larger fraction of events than the accidentals is $(\tau_\beta + \Delta t_{\beta\gamma})$ where $\Delta t_{\beta\gamma}$ is the mean time difference between correlated β and γ signals for a given γ channel. The identification of events in the plateau was checked by studying triple coincidence events and comparing the results with expectations based on the detector efficiencies. It was further tested by studying the decay time of such events. Because the rate of uncorrelated events from two decays occurring during the dead-time window varies quadratically with the rate, their decay time is expected to be half the decay time of ^{20}F. This was confirmed by fitting the decay curve obtained when setting a time window on the plateau of Fig. 9. The contribution of such events has therefore an important impact on the extracted half-life. Because of the relatively low rate in the γ detectors, the pile-up with signals from ambient background, which are also uncorrelated in time, has a much smaller contribution.

To estimate the systematic effect from the presence of such uncorrelated events, the width of the time window used on the relative time spectra (Fig. 6) was increased by more than a factor of 10, increasing thereby also the amount of such events. It is clear from Figs. 6 and 9 that the number of prompt events remains the same when increasing the window around the peak. The variation of the half-life as a function of the half-width of the time window is shown in Fig. 10. The narrowest window, with ±24 ns cuts around the peak used in the analysis, still contains a small fraction of such uncorrelated coincidences. The extrapolation to zero of the variation trend of the half-life gives then the size of the correction, of 1.47 ms. Because this correction also depends on the lower cut on the β energy spectrum, its uncertainty is conservatively taken as the value of the correction.

It is observed from Fig. 10 that the pile-up events tend to decrease the half-life because, as explained above, their rate varies quadratically with the decay rate of ^{20}F. A set-by-set analysis confirmed that the effect is smaller for set 3 than for sets 4–7, as expected. It is to note that the procedure described above also corrects for uncorrelated events from ambient background (Sec. VI D) which are evenly distributed in the time coincidence spectrum of Fig. 9. The combined systematic effect was therefore labeled "Uncorrelated events" in Table IV.

D. Background

The γ-energy cut (Fig. 4) can potentially allow the detection of background events. As mentioned above, two other

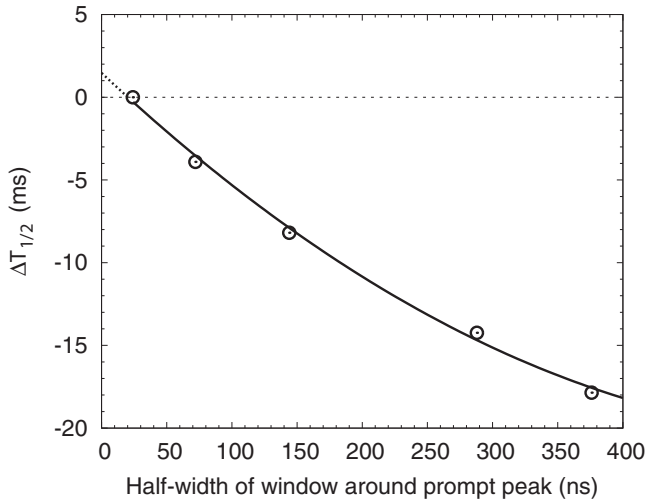

FIG. 10. Systematic variation of the half-life obtained from sets 3–7 as a function of half the width of the window used as cut around the prompt peak in the time difference spectra (Fig. 6). The value obtained for 24 ns is taken as reference. The circles show the difference between the average value resulting from the fits and the value obtained for 24 ns. The solid black line is a quadratic description of the variation. The extrapolation to zero width (dotted line) gives the size of the correction.

visible contributions in the 1.63-MeV peak window arise from bremsstrahlung events, extending towards higher energies, and from Compton events, from the detector resolution. Both types of $\beta\gamma$ events produce prompt coincidences and they have, furthermore, the same time signature as the main $\beta\gamma$ events in the 1.63-MeV peak.

The lowest background level in the time decay spectrum is determined by the contribution of accidental coincidences from ambient background. It is delicate to determine such level of accidentals in the decay spectrum by adding another free parameter to the fit function in Eq. (1) because of the correlations with the half-life and with the initial activity. To reduce the correlations, an attempt was made to simultaneously fit all four decay spectra from a single run using a function of the form,

$$g_i(t) = a_i[\exp(-t \ln 2/T_{1/2}) + r_i], \tag{3}$$

where a_i and r_i are free parameters for each decay spectrum but $T_{1/2}$ is a free parameter common to all spectra. Such a constraint reduces the correlations between parameters for a given detector but introduces correlations between the detectors. The results from such analysis showed that the individual values of the parameters r_i are statistically consistent with zero and that for the Left, Right, and Down detectors there was a comparable amount of negative and positive central values of these parameters. For the Up detector, the fraction of positive values was larger than that of negative values, consistent with the fact that the half-life for this detector is observed to be larger when the background was assumed to be zero (Table III), and consistent also with the correlation with the other three detectors, which drive the value of the fitted half-life.

A similar analysis using Eq. (3) was performed on sets of simulated data to study the sensitivity of such a procedure to the background level and to confirm the correlations and the statistical impact observed in the experimental data. The result showed that it is not possible to obtain a precise determination of the background level over the relatively short decay window, for each detector and for each run, when such level is too small.

Alternatively, the level of accidental background can be independently measured for each detector by considering the events located left from the prompt peak in Fig. 9. The analysis of all decay spectra was then performed by determining first the background level from those events in the time difference spectrum and then fixing this level in the fitted function. This analysis showed that the systematic error made by assuming no background in the fitting function of Eq. (1) was 0.2 ms when using the ±24-ns time cuts on the time difference spectrum. The analysis also showed that, on average, for the same time window on the relative time spectrum, the amplitude of the accidental background relative to the initial activity in the decay spectrum is 7.6×10^{-6}. This is one of the major advantages of the measurement described here. Although the measurement is performed over a relatively short time window, the level of accidental background is very low because of the coincidence condition.

The studies described above are useful to understand the effect of the ambient background separated from the pile-up. As discussed in Sec. VI C, the correction from the time uncorrelated events shown in Fig. 10 includes both the pile-up events, which give rise to the plateau right from the prompt peak, as well as the accidental background events, which are uniformly distributed. Their effects on the half-life have opposite signs but the pile-up events produce an effect which is a factor of 8 larger, consistent with their distribution in Fig. 9. It is therefore not necessary to add an independent correction and an associated uncertainty because of the level of accidental background.

E. Gain drifts

The amplitudes of the PVT signals induced by the LED were inspected during the decay window. For sets 1 and 2 of Table I, for which the HV inhibit was not active, the LED-induced signals showed a relative gain drift of 4.8×10^{-3} over the 30-s decay. This is reduced to 3.8×10^{-4} in the sets where the HV inhibit was active. Figure 11 shows the variation of the pulser amplitudes for two runs, one with the inhibit OFF (upper panel) and one with the inhibit ON (lower panel).

Because of the fixed lower cut on the PVT spectrum, the presence of this time-correlated gain increase results in a larger fraction of the energy spectrum being counted at later times, producing a systematically larger half-life.

When using the lowest position of the lower cut in the PVT energy spectrum (Fig. 5), the results obtained from sets 1 and 2 do not display a significant difference in the values compared to the other sets (Table II). However, varying the lower cut in the PVT energy has a significantly larger impact on the results from sets 1 and 2, which cover run numbers up to 254 included, than for the runs in the other sets. These systematic changes in sets 1 and 2 are consistent with the measured gain drift.

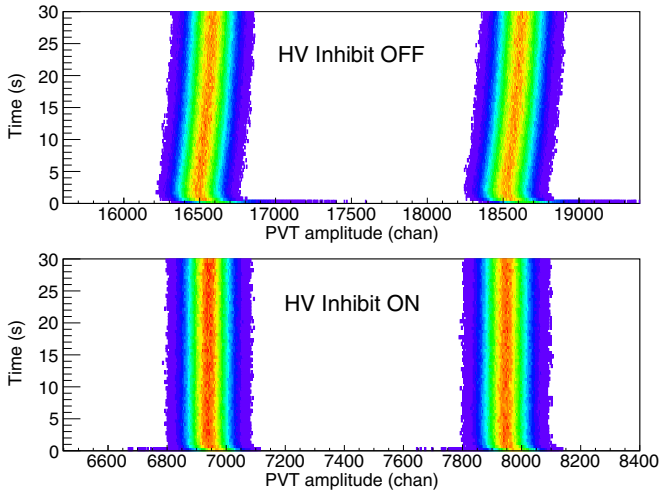

FIG. 11. Variation of the amplitude of the two pulser signals during the decay time. (Upper panel) Variation observed in a run from set 1 for which the HV inhibit was OFF. (Lower panel) Variation from a run from set 5 with the HV inhibit ON. The horizontal scales have been adjusted so that the relative positions and widths of the distributions are similar.

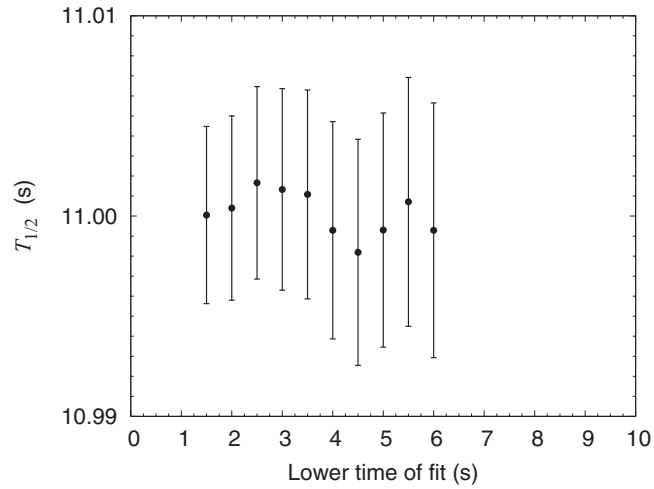

FIG. 12. Mean value of the half-life obtained from the fits of the decay spectra as a function of the lower time of the fit. The error bars display only the statistical uncertainty.

In principle it is possible to correct for this effect using the pulser information. Such a procedure would anyway result in a larger uncertainty for these sets and we have opted to exclude sets 1 and 2 from the data to extract the final result.

F. Sensitivity to cuts

The cuts on the CsI(Na) energy (Fig. 4) were defined such as to reduce the sensitivity to possible gain drifts. Off-line measurements have shown that, for the rate variations measured by the CsI(Na) detectors during the decay, the effect of rate-correlated gain drifts is negligible. The lower and upper cuts on the CsI(Na) detectors were independently varied by ± 5 keV, corresponding to a rate correlated gain variation which is 10 times larger than expected for the actually measured rates.

For the PVT detector, the upper cut on the energy distribution was set sufficiently high with respect to the main β spectrum and the pile-up events, and below the position of the LED pulser signals (Fig. 5). The lower cut in the PVT energy is the most sensitive of all cuts and, as mentioned above, was found to produce a systematic trend for sets 1 and 2, consistent with the observed gain drift.

For lower cuts ranging from above the ^{10,11}C contaminants up to the middle of the β spectrum, there was no significant trend observed in the values of the half-life for sets 3–7. For the final analysis, the lower PVT energy cut was set at the lowest end of this range. The systematic uncertainty associated with the variation of the lower PVT cut was taken as the maximal variations on the half-life observed for sets 3–7, and was ± 2.32 ms.

For the decay histograms, the lower 24 and upper 24 bins, which span 6 s on each side, were independently removed. No systematic trend was observed in the variation of the central values. For illustration, Fig. 12 shows the values of the half-life as a function of the starting time of the fit, indicating no systematic trend of the central values with rate.

G. Binning and fitting method

The fits have been performed using log-likelihood estimators on summed data. Two independent analysis were performed using methods from two packages: PHYSICA [21] and ROOT, Version 6.04. When applied to the same data, the two methods gave identical results. The ROOT methods have been tested with simulated data, having comparable statistics, fitting range, and binning as those used for the experimental data. The PHYSICA methods were also tested with experimental data, by comparing the result from the fit of a summed histogram with the result from the analytic solution of the maximum likelihood estimator for the lifetime, calculated with unbinned events from the data stream. The analytic solution is given by the sample mean corrected by the finite time of the measuring window. No bias in the minimization methods at the current level of precision was found. The stability of the results was also tested as a function of the binning of the decay histogram. The final central value changed by -0.6 ms when the number of bins was reduced by a factor of 2, consistent with Monte Carlo simulations. This was included in the list of systematic effects with a correction of -0.3 ms and a systematic uncertainty of 0.3 ms.

H. ^{20}F Diffusion

Any process reducing the number of nuclei in the sample with time, other than β decay, will result in a shorter half-life. We have considered the possibility of F diffusion out of the PVT. It is difficult to find Arrhenius coefficients which closely correspond to actual experimental conditions, with F atoms implanted in polyvinyltoluene at room temperature. Based on fluorination work of fluorine gas in other polymer films [22] it was estimated that in 30 s, the root mean square radial displacement is about 0.75 μm. This estimate indicates that diffusion effects are negligible.

TABLE V. Values of the ^{20}F half-life obtained in previous measurements along with the result from this work. The "label" in the second column refers to those used in Figs. 1 and 13.

$T_{1/2}$ (s)	Label (year) Ref.
11.56(5)	Mal (1962) [15]
11.36(7)	Gli (1963) [12]
10.31(7)	Yul (1967) [13]
11.03(6)	Wil (1970) [2]
10.996(20)	Alb (1975) [10]
11.18(1)	Gen (1976) [9]
11.03(6)	Min (1987) [11]
11.163(8)	Wan (1992) [8]
11.11(4)	Ito (1995) [14]
11.0011(75)	This work

VII. RESULT AND DISCUSSION

With the scaling of the statistical uncertainty of the result from Table III and the total systematic correction and error listed in Table IV, the final result from this measurement is

$$T_{1/2} = 11.0011(69)_{\text{stat}}(30)_{\text{sys}}\text{s}, \tag{4}$$

and is listed along with previous results in Table V. This value is consistent with those from Wilkinson and Alburger [2] and from Minamisono [11], which are identical, and is also consistent with the value from Alburger and Calaprice [10]. The weighted mean of the two most precise results [8,9], which are mutually consistent and dominate the current value, gives $T_{1/2} = 11.1696(62)$ s. The value in Eq. (4) is at variance by 17 combined standard deviations from this weighted mean. The impact of the value obtained from the present work on the set of available results is shown in Fig. 13 and is to be compared with the prevailing situation shown in Fig. 1.

It is difficult to comment on eight among the nine previously published results because they do not contain detailed accounts of the measuring conditions and data analysis. Only Wang *et al.* [8] performed a dedicated measurement that attempted to resolve the then existing discrepancies. It is intriguing that the uncertainties quoted there for the half-life (Table 1 of Ref. [8]) are almost identical when the background was either floating or fixed in the fits. When adding a constant background as a free parameter, the correlation between this parameter and the half-life increases the statistical uncertainty on the half-life parameter. A simulation of decay spectra with similar conditions to those described in Ref. [8] showed that the uncertainty on the half-life increases by a factor of about 5 when the background parameter is left free as compared to when it is fixed in the fits. Even though the discussion lists a number of systematic effects, the uncertainty quoted in Ref. [8] is purely statistical.

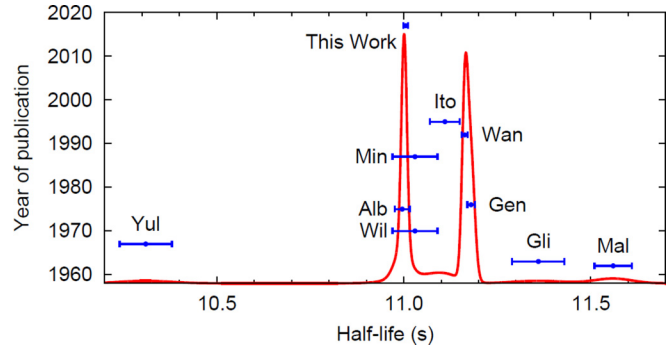

FIG. 13. Measurements of the ^{20}F half-life including the result from the present work. See caption of Fig. 1 for details.

VIII. CONCLUSION

Nine values of the ^{20}F half-life have been reported in the literature for which the uncertainty is at most 10 times larger than the most precise result. For eight of them the information about the experimental conditions and the data analysis is somewhat scarce. The measurement of Wang *et al.* [8] aimed at resolving existing discrepancies among previously published results. The present work reported a new measurement of the half-life by counting $\beta\gamma$ coincidences with a digital data acquisition system which recorded the energies and the time stamps. Two major advantages of the technique used here are (i) the dead time of the counting channels were smaller than 660 ns and (ii) the level of accidental coincidences from ambient background relative to the initial activity was smaller than 8×10^{-6}. A detailed description of the experimental conditions, of the data analysis, and of systematic effects was given. The weight of the value obtained here revives the poor consistency among existing results by adding tension with the most precise results. This calls for a new measurement of the half-life, with a technique having different sources of systematic effects, to clarify the discrepancy.

ACKNOWLEDGMENTS

We thank M. Brodeur and X. Fléchard for fruitful discussions and T. Chuna for his assistance during the experiment. This work was supported by the National Science Foundation under Grants No. PHY-1102511, No. PHY-1506084, and No. PHY-1565546.

[1] L. Grenacs, Annu. Rev. Nucl. Part. Sci. **35**, 455 (1985).
[2] D. H. Wilkinson and D. E. Alburger, Phys. Rev. Lett. **24**, 1134 (1970).
[3] K. Nomoto, C. Kobayashi, and N. Tominaga, Annu. Rev. Astron. Astrophys. **51**, 457 (2013).
[4] K. Langanke and G. Martínez-Pinedo, Nucl. Phys. A **928**, 305 (2014).
[5] G. Martínez-Pinedo, Y. H. Lam, K. Langanke, R. G. T. Zegers, and C. Sullivan, Phys. Rev. C **89**, 045806 (2014).

[6] L. Hayen, N. Severijns, K. Bodek, D. Rozpedzik, and X. Mougeot, Rev. Mod. Phys. **90**, 015008 (2018).
[7] D. R. Tilley, C. M. Cheves, J. H. Kelley, S. Raman, and H. R. Weller, Nucl. Phys. A **636**, 249 (1998).
[8] T. F. Wang, R. N. Boyd, G. J. Mathews, M. L. Roberts, K. E. Sale, M. M. Farrell, M. S. Islam, and G. W. Kolnicki, Nucl. Phys. A **536**, 159 (1992).
[9] H. Genz, A. Richter, B. M. Schmitz, and H. Behrens, Nucl. Phys. A **267**, 13 (1976).
[10] D. E. Alburger and F. P. Calaprice, Phys. Rev. C **12**, 1690 (1975).
[11] T. Minamisono, Hyperfine Interact. **35**, 979 (1987).
[12] S. S. Glickstein and R. G. Winter, Phys. Rev. **129**, 1281 (1963).
[13] H. P. Yule, Nucl. Phys. A **94**, 442 (1967).
[14] S. Itoh, M. Yasuda, H. Yamamoto, T. Iida, A. Takahashi, and K. Kawade, in *1994 Symposium on Nuclear Data* (Tokai, Japan, 1995).
[15] S. Malmskog and J. Konijn, Nucl. Phys. **38**, 196 (1962).
[16] M. Hughes, O. Naviliat-Cuncic, P. Voytas, E. George, and X. Huyan, Bull. Am. Phys. Soc. **62**, S13.00004 (2017).
[17] D. J. Morrissey, B. M. Sherrill, M. Steiner, A. Stolz, and I. Wiedenhoever, Nucl. Instrum. Methods Phys. Res., Sect. B **204**, 90 (2003).
[18] D. Weisshaar, A. Gade, T. Glasmacher, G. F. Grinyer, D. Bazin, P. Adrich, T. Baugher, J. M. Cook, C. A. Diget, S. McDaniel, A. Ratkiewicz, K. P. Siwek, and K. A. Walsh, Nucl. Instrum. Methods Phys. Res., Sect. A **624**, 615 (2010).
[19] O. B. Tarasov and D. Bazin, Nucl. Instrum. Methods Phys. Res., Sect. B **376**, 185 (2016).
[20] C. J. Prokop, S. N. Liddick, B. L. Abromeit, A. T. Chemey, N. R. Larson, S. Suchyta, and J. R. Tompkins, Nucl. Instrum. Methods Phys. Res., Sect. A **741**, 163 (2014).
[21] http://computing.triumf.ca/legacy/physica/.
[22] J. Shimada and M. Hoshino, J. Appl. Polym. Sci. **19**, 1439 (1975).